SCIENTIFIC REPORTS

OPEN

SUBJECT AREAS:
BATTERIES
ELECTROCATALYSIS

Received
14 May 2014

Accepted
24 June 2014

Published
14 July 2014

Correspondence and requests for materials should be addressed to N.M. (tmizuno@mail.ecc.u-tokyo.ac.jp)

A New Sealed Lithium-Peroxide Battery with a Co-Doped Li_2O Cathode in a Superconcentrated Lithium Bis(fluorosulfonyl)amide Electrolyte

Shin-ichi Okuoka[1], Yoshiyuki Ogasawara[2], Yosuke Suga[2], Mitsuhiro Hibino[2], Tetsuichi Kudo[2], Hironobu Ono[1], Koji Yonehara[1], Yasutaka Sumida[1], Yuki Yamada[3], Atsuo Yamada[3], Masaharu Oshima[4], Eita Tochigi[5], Naoya Shibata[5], Yuichi Ikuhara[5] & Noritaka Mizuno[2]

[1]Advanced Materials Research Center, Nippon Shokubai Co., Ltd. 5-8, Nishi Otabi-cho, Suita, Osaka, Japan, [2]Department of Applied Chemistry, School of Engineering, The University of Tokyo, 7-3-1 Hongo, Bunkyo-ku, Tokyo, Japan, [3]Department of Chemical System Engineering, School of Engineering, The University of Tokyo, 7-3-1 Hongo, Bunkyo-ku, Tokyo, Japan, [4]Synchrotron Radiation Research Organization, The University of Tokyo, 7-3-1 Hongo, Bunkyo-ku, Tokyo, Japan, [5]Institute of Engineering Innovation, School of Engineering, The University of Tokyo, 2-11-16 Yayoi, Bunkyo-ku, Tokyo, Japan.

We propose a new sealed battery operating on a redox reaction between an oxide (O^{2-}) and a peroxide (O_2^{2-}) with its theoretical specific energy of 2570 Wh kg^{-1} (897 mAh g^{-1}, 2.87 V) and demonstrate that a Co-doped Li_2O cathode exhibits a reversible capacity over 190 mAh g^{-1}, a high rate capability, and a good cyclability with a superconcentrated lithium bis(fluorosulfonyl)amide electrolyte in acetonitrile. The reversible capacity is largely dominated by the O^{2-}/O_2^{2-} redox reaction between oxide and peroxide with some contribution of the Co^{2+}/Co^{3+} redox reaction.

Rechargeable lithium ion batteries (LIBs) operating on shuttling of lithium between the negative and positive electrodes, both of which are composed of topotactic insertion hosts of lithium such as graphite and $LiCoO_2$, are indispensable to our society as power sources for portable and large electronic appliances such as notebook computers and electric vehicles. However, their energy densities are rather modest; even the state-of-the-art LIBs do not exceed 250 Wh kg^{-1}. Therefore, various researches are being carried out to develop post-LIBs with much higher energy densities.

One of the approaches is utilization of electrode materials operating on so-called conversion reactions and the theoretical specific capacity is 714 mAh g^{-1} for the reaction of $CoO + 2Li^+ + 2e^- \rightarrow Co + Li_2O$[1], while the severe hysteresis in voltage between the charging and discharging processes generally limits the energy efficiency. Moreover, some metal oxides including CoO show surprisingly good cycling reversibility despite the highly destructive nature of the conversion reaction. However, such oxide materials can be used only for anodes, because their working potentials are typically in the range of 0–1 V (vs. Li/Li^+) and low. Recently, some fluorides such as BiF_3[2] and FeF_2 (or FeF_3)[3] have been reported to operate at higher potentials (2.7–3.4 V), while their poor kinetics and reversibility are problems.

Another approach is a development of a lithium-air (Li-O_2) battery by use of atmospheric O_2 with a theoretical specific energy of 3400 Wh kg^{-1} even including the weight of oxygen in the discharged product (Li_2O_2). However, the actual capacity or the energy is dependent on the pore volumes of the cathode matrices where Li_2O_2 is formed, the pores are clogged with solids, and the discharge is prohibited by the limitation of the oxygen supply. In addition, there are more serious inherent problems of the open device, suffering from the coexisting moisture and CO_2, and safety for the application to electronic vehicles. The main discharge product for Li-O_2 batteries is Li_2O_2 according to the reaction (the equilibrium potential, E° (vs. Li/Li^+))[4,5],

$$O_2 + 2Li^+ + 2e^- \rightarrow Li_2O_2 \left(E_1^\circ = 2.96\ \text{V}\right). \quad (1)$$

The subsequent reduction of Li_2O_2 has recently been pointed out to take place to form Li_2O during the deep discharge according to the reaction[6–9],

$$Li_2O_2 + 2Li^+ + 2e^- \rightarrow 2Li_2O \left(E_2^\circ = 2.87\ V\right). \quad (2)$$

However, there is no report on the repetition of the charge and discharge utilizing the reaction between Li_2O (or O^{2-}) and Li_2O_2 (or O_2^{2-}). The investigation on LIB cathodes such as $LiCoO_2$ and Li-rich layered oxides shows not only the charge compensation mechanism involving transition metal ions but also some contribution of the reversible redox reaction of oxygen atoms[10–13]. Therefore, we have reached an idea that Li_2O_2 would act as a 3 V-level cathode utilizing the redox couple of oxide (O^{2-})/peroxide (O_2^{2-}) [equation (2)]. In addition, a certain electrode catalyst or mediator would selectively accelerate the thermodynamically more favourable backward reaction of equation (2) instead of the backward reaction of equation (1) and the following reaction,

$$Li_2O \rightarrow 1/2O_2 + 2Li^+ + 2e^- \left(E_3^\circ = 2.91\ V\right). \quad (3)$$

Here, we propose a new sealed battery operating on a redox reaction between O^{2-} and O_2^{2-} with its theoretical specific energy of 2570 Wh kg^{-1} (897 mAh g^{-1}, 2.87 V, see the Supplementary Information) based on the reaction,

$$2Li + Li_2O_2 \rightarrow 2Li_2O, \quad (4)$$

and demonstrate that a Co-doped Li_2O cathode exhibits a reversible capacity over 190 mAh g^{-1}, a high rate capability, and a good cyclability with a superconcentrated lithium bis(fluorosulfonyl)amide (LiFSA) electrolyte in acetonitrile[14]. The reversible capacity is largely dominated by the reaction of equation (2) with some contribution of the redox reaction of Co ions.

Results

Preparation and Characterization of the Co-Doped Li_2O Cathode. The powders (Co/Li = 0.025–0.2) of Li_2O and Co_3O_4 were pulverized and the Co-doped Li_2O were obtained. Among them, the Co-doped Li_2O (Co/Li = 0.1) showed the best charge-discharge performance (Supplementary Figure S1a). The electronic conductivity of the Co-doped Li_2O (Co/Li = 0.1) powder compact was 5.3×10^2 kΩ cm, while Li_2O is an insulator. Therefore, the resulting Co-doped Li_2O (Co/Li = 0.1) was hereafter used as a cathode and the specific capacity was calculated on the basis of the total weight of the Co-doped Li_2O. Rh_2O_3 and IrO_2 could also act similarly to Co_3O_4 (Supplementary Figure S1b).

In the X-ray diffraction (XRD) pattern of the Co-doped Li_2O (Supplementary Figure S2), broad peaks of anti-fluorite-type Li_2O and a weak peak at 44.8° of cubic $LiCoO_2$[15] were observed, while peaks of spinel-type Co_3O_4 were not observed. The peak intensity of the cubic $LiCoO_2$ increased upon increase in the Co/Li ratio.

The Co K-edge X-ray absorption near edge structure (XANES) measurement of the Co-doped Li_2O was carried out to investigate the oxidation states and coordination environments of the Co species (Supplementary Figure S3). The absorption edge position agreed with that of starting Co_3O_4, indicating that the average Co valence does not change under mechanical milling conditions. The pre-edge peak of the Co-doped Li_2O was stronger than those of Co_3O_4 and $LiCoO_2$ and as strong as that of the spinel $CoAl_2O_4$, in which every Co^{2+} ion is located at the tetrahedral site. This absorption represents the transition of the 1s electron to an unoccupied d orbital of Co ions, which is an electric dipole forbidden transition in an ideal octahedral symmetry, while the noncentrosymmetric tetrahedral environment allows the transition[16,17]. Thus, the intense pre-edge peak shows the presence of considerable amounts of tetrahedral Co.

Electrochemical Performance. The charge and discharge curves of the cell consisting of the Co-doped Li_2O cathode, a Li metal anode, and a superconcentrated 4 M LiFSA electrolyte in acetonitrile[14] are shown in Figure 1. The charge voltage gradually increased and reached approximately 3.2 V above 150 mAh g^{-1}. The discharge and charge curves from the first to 15th cycle almost unchanged with the constant coulombic efficiency of *ca.* 96% at 45 mA g^{-1} (Figure 1a). The 1st discharge capacity reached 195 mAh g^{-1} at a low current density of 13.5 mA g^{-1} and the capacity of 133 mAh g^{-1} can be discharged even at a very high current density of 1080 mA g^{-1} at which the capacity of 200 mAh g^{-1} can be charged in 11 min (Figure 1b).

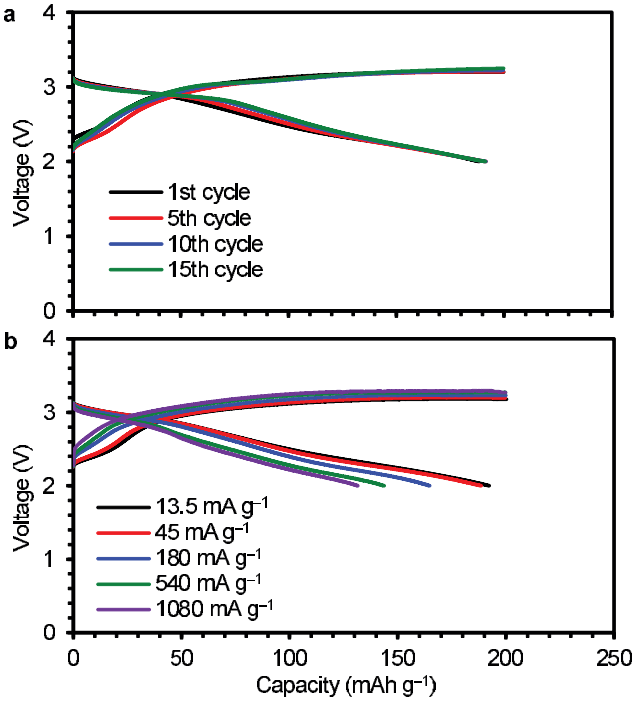

Figure 1 | Electrochemical performances of the Co-doped Li_2O cathode. (a) Charge and discharge voltage curves in repeated charge/discharge cycles at 45 mA g^{-1}. (b) Charge and discharge voltage curves at various current densities (13.5–1080 mA g^{-1}). Each testing cell was charged to 200 mAh g^{-1}, and then discharged to the cut off voltage of 2.0 V at a constant current density.

Co K-edge XANES Measurement of the Co-Doped Li_2O Cathode during the Charge and Discharge Process. The Co K-edge XANES spectra were measured at various charge and discharge capacities (Figure 2). In the charge process from 0 to 54 mAh g^{-1}, the absorption edge position shifted to the higher photon energy, indicating the oxidation of Co^{2+} to Co^{3+}. By the further increase in the capacity the edge position of Co^{3+} did not change. In the discharge process after the charge to 270 mAh g^{-1}, the absorption edge position hardly changed in the range of 0–162 mAh g^{-1} and then returned to the initial position upon the discharge to 250 mAh g^{-1}.

Peroxide Analysis in the Co-Doped Li_2O Cathode during the Charge and Discharge Process. We quantified O_2^{2-} species in the Co-doped Li_2O cathode at various charge and discharge capacities. Figure 3a shows the amounts of the O_2^{2-} (detected as O_2) in the cathode at various charge capacities. In the range of 0–54 mAh g^{-1}, the amounts of the O_2^{2-} were negligible. In the region 54–216 mAh g^{-1}, the amounts of the O_2^{2-} increased and the slope from 162 mAh g^{-1} to 216 mAh g^{-1} corresponded to 0.5 O_2^{2-}/e^-. In the final region of 216–270 mAh g^{-1}, the amounts of the O_2^{2-} more gradually increased.

Figure 3d shows amounts of the O_2^{2-} in the cathode at various discharge capacities after the charge to 270 mAh g^{-1}. In the region of 0–162 mAh g^{-1}, the amounts of the O_2^{2-} decreased and the slope from 0 mAh g^{-1} to 108 mAh g^{-1} corresponded to 0.5 O_2^{2-}/e^-. In the

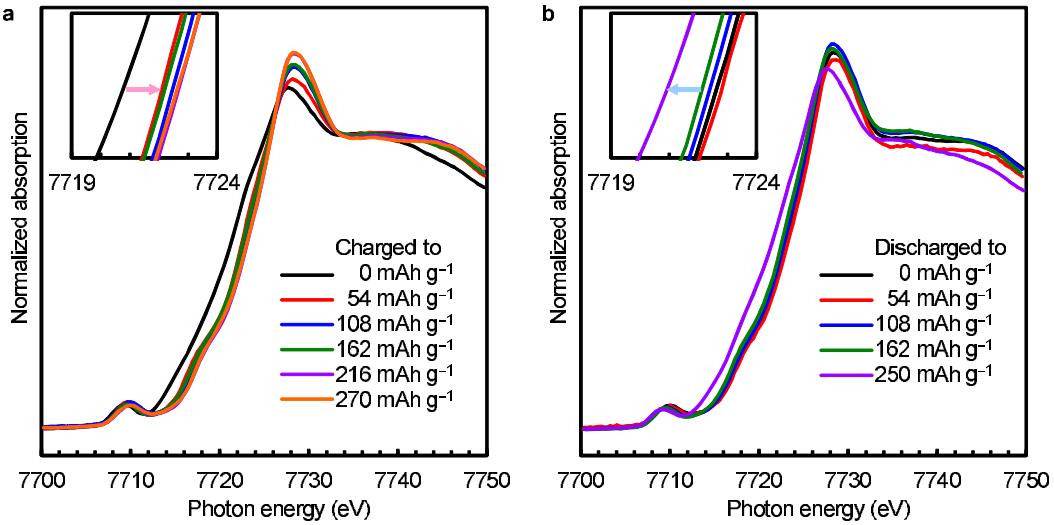

Figure 2 | Co K-edge XANES spectra of the Co-doped Li_2O cathode at various charge and discharge capacities. The current densities were 4.5 mA g^{-1}. The insets show the absorption edge regions of the spectra. (a) Charge process. (b) Discharge process.

final region of 162–250 mAh g^{-1}, the O_2^{2-} was hardly detected. We also quantified the O_2^{2-} species in the cathode recharged to 270 mAh g^{-1}. The amount of the O_2^{2-} was 2.31 mmol g^{-1} in approximate agreement with that for the first charge.

Observation and Analysis of the Cathode during the Charge. The in-situ gas phase analysis during the charge process was conducted. In Figure 4b, cumulative amounts (per weight of the Co-doped Li_2O cathode) of O_2 and CO_2 evolved are shown together with its charge curve (Figure 4a). In the range of 0–216 mAh g^{-1}, O_2 was hardly observed, and then the amount of O_2 evolution monotonically increased. The slope of O_2 evolution in the range of 324–594 mAh g^{-1} almost corresponded to 0.25 O_2/e^-. The XRD 111 peak intensity of the Co-doped Li_2O was approximately linearly weakened with increase in the charge capacity from 0 to 324 mAh g^{-1} and was more slowly weakened at 540 and 580 mAh g^{-1} (Figure 4c and

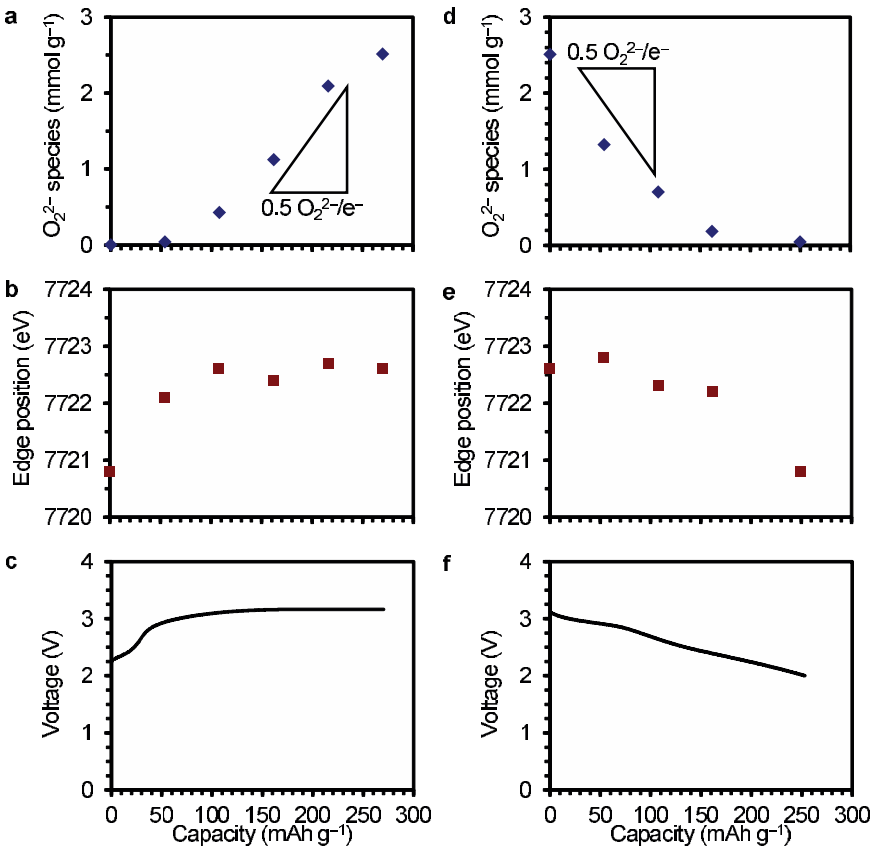

Figure 3 | Analysis of the Co-doped Li_2O cathodes after the charge and the discharge. (a) and (d) Analytical peroxide amounts of the cathodes after the charge (a) and discharge (d). (b) and (e) Co K-edge XANES absorption edge positions of the cathodes after the charge (b) and discharge (e). (c) and (f) Charge (c) and discharge (f) voltage curves at current density of 4.5 mA g^{-1}.

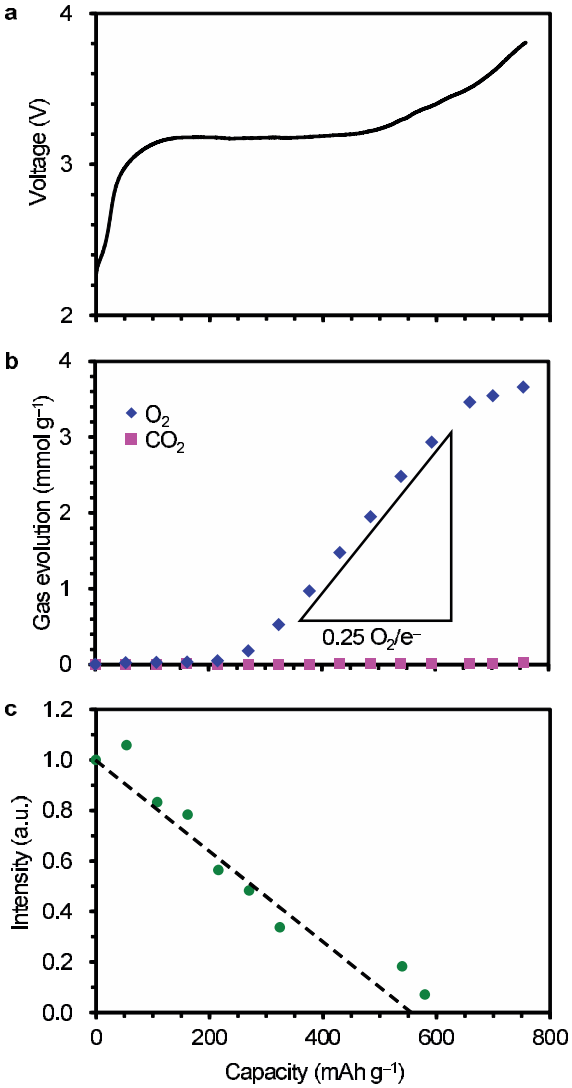

Figure 4 | Voltage, gas evolution, XRD peak intensity of the Co-doped Li_2O cathode in the charge process. (a) The voltage curve. (b) Cumulative amounts of O_2 and CO_2 evolved in the charge process at the current density of 4.5 mA g^{-1}. The slope of 0.25 O_2/e^- indicates theoretical rate of O_2 evolution according to the reaction, $2O^{2-} \rightarrow 4e^- + O_2$. (c) The XRD 111 peak intensity of Co-doped Li_2O. The peak intensity at 0 mAh g^{-1} was taken as a unity. The black line is a theoretical line of change in the peak intensity.

Supplementary Figure S4). The evolution of CO_2 was not observed in the whole range of the charge process.

Direct observation of the Co-doped Li_2O cathode charged to 270 mAh g^{-1} was attempted with high resolution transmission electron microscopy (HRTEM). Figure 5 shows the HRTEM image and the fast Fourier transform (FFT) pattern. Since some spots in Figure 5b lie on the circles estimated with the Li_2O_2 crystal structure, many fringe regions surrounded by red circles in Figure 5a are likely attributable to Li_2O_2. In contrast, for the starting cathode before the charge, since all spots (Supplementary Figure S5b) lie on the circles estimated with Li_2O or cubic $LiCoO_2$ crystal structures, many fringe regions surrounded by red circles (Supplementary Figure S5a) are likely attributable to Li_2O or cubic $LiCoO_2$.

Discussion

Upon increase in Co content above Co/Li = 0.1, the discharge capacity decreased (Supplementary Figure S1a) and the XRD peak intensity of cubic $LiCoO_2$ increased (Supplementary Figure S2), suggesting

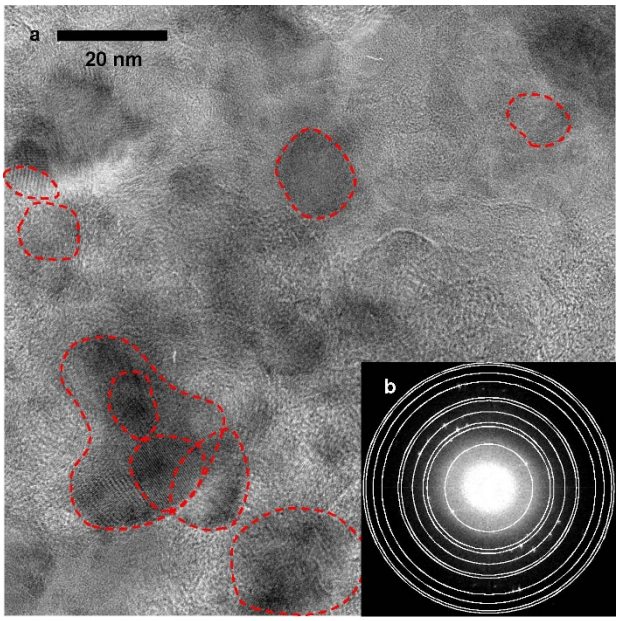

Figure 5 | HRTEM image and FFT pattern of the Co-doped Li_2O. (a) HRTEM image after the charge. The areas in red circles were obtained by the inverse Fourier transformation of the spots in the FFT pattern that are attributed to Li_2O_2. The periods of the fringe in the areas were confirmed to be equal to those in Li_2O_2. (b) FFT pattern of the HRTEM image. The white circles are on the basis of Li_2O_2.

that the resulting cubic $LiCoO_2$ is inactive for the charge and discharge reactions at the voltage of 2.0–3.2 V (vs. Li/Li^+) as has been reported in ref. (18).

In the XRD pattern of the Co-doped Li_2O (Supplementary Figure S2), broad peaks of anti-fluorite-type Li_2O and a weak peak at 44.8° of cubic $LiCoO_2$[15] were observed, while peaks of spinel-type Co_3O_4 were not observed. The volume fractions of Co-doped Li_2O and cubic $LiCoO_2$ were estimated to be 0.90 : 0.10 with the parameters of 111 reflection of Co-doped Li_2O and 200 one of cubic $LiCoO_2$ in Supplementary Table S1 (see the Supplementary Information). The Co K-edge XANES spectrum of the Co-doped Li_2O shows the presence of considerable amounts of tetrahedral Co (Supplementary Figure S3). These results indicate that most of Co ions are substitutionally doped in the tetrahedral Li sites of the anti-fluorite Li_2O structure with formation of vacancies at the same sites due to charge compensation. Co^{2+} and Co^{3+} in the Co-doped Li_2O would be randomly distributed at the tetrahedral sites in a defective anti-fluorite structure, since the XRD pattern was not identical to that of the defective anti-fluorite structure, in which Co ions were ordered in the tetrahedral sites[19,20].

The Co-doped Li_2O cathode, of which the theoretical specific capacity is calculated to be 556 mAh g^{-1} based on the weight of Li_2O in the Co-doped Li_2O (see the Supplementary Information), exhibited a reversible capacity over 190 mAh g^{-1}, a high rate capability, and a good cyclability (Figure 1). The electronic conductivity of the Co-doped Li_2O powder compact was 5.3×10^2 kΩ cm and of the same level (5×10^2 kΩ cm) as that of $LiMn_2O_4$[21], showing that the Co-doped Li_2O can work as an electrode material. This conductivity is possibly explained by narrowing of the Li_2O band gap by formation of the impurity state with the dope of Co or becoming metallic by the carrier dope. The coulombic efficiency of the present system is 96% and still below 100%. This is possibly explained by the progress of the side reaction of solid electrolyte interface formation during the charge other than CO_2 formation.

To clarify the oxidation states of Co and the presence of O_2^{2-} in the Co-doped Li_2O cathode, the Co K-edge XANES measurement and

quantification of O_2^{2-} species were carried out at various charge and discharge capacities (Figures 2 and 3). In the charge process from 0 to 54 mAh g^{-1}, the oxidation of Co^{2+} to Co^{3+} proceeds without the O^{2-} oxidation (Figures 3a and 3b). The oxidation of Co^{2+} to Co^{3+} in the charge process is completed at the charge capacity ≤54 mAh g^{-1} in accord with the theoretical capacity (39 mAh g^{-1}) of the cathode due to the oxidation of Co^{2+} to Co^{3+}. In the region of 54–216 mAh g^{-1}, the amounts of the O_2^{2-} increased and the slope from 162 mAh g^{-1} to 216 mAh g^{-1} corresponded to 0.5 O_2^{2-}/e^-, suggesting the O_2^{2-} formation according to the backward reaction of equation (2) (Figure 3a). In the final region of 216–270 mAh g^{-1}, the amounts of the O_2^{2-} more gradually increased. Considering the O_2 evolution curve (Figure 4b), both the O_2^{2-} formation and O_2 evolution reactions likely proceed in this region.

In the discharge process from 0 to 162 mAh g^{-1}, the amounts of the O_2^{2-} decreased and the slope from 0 mAh g^{-1} to 108 mAh g^{-1} corresponded to 0.5 O_2^{2-}/e^-, suggesting the consumption of the O_2^{2-} according to equation (2) (Figure 3d). In the final region of 162–250 mAh g^{-1}, the O_2^{2-} was hardly detected, indicating that the discharge mostly consists of the reduction of Co^{3+} to Co^{2+}, in agreement with the Co K-edge XANES results (Figures 2b and 3e). In the recharge process to 270 mAh g^{-1}, the amount of the O_2^{2-} was 2.31 mmol g^{-1} in approximate agreement with that for the first charge, suggesting reversible formation of O_2^{2-} in the repeated cycles.

It is essentially important for the present battery that no substantial amount of O_2 is released in the charge process. Moreover, CO_2 evolution accompanied by anodic side reactions between Li_2O_2 and carbon additives or electrolytes has been pointed out as a problem of the Li-O_2 batteries[22–24]. In the range of 0–216 mAh g^{-1}, O_2 was hardly observed (Figure 4b), suggesting that the side reactions of O_2 evolution do not proceed and Co-doped Li_2O is oxidized according to the reaction, $2O^{2-} \rightarrow O_2^{2-} + 2e^-$, with some contribution of the oxidation of Co ions. The slope of 0.25 O_2/e^- in the range of 324–594 mAh g^{-1} suggests that O_2 is formed according to the direct reaction (i) $2Li_2O \rightarrow O_2 + 4Li^+ + 4e^-$ and/or the consecutive reaction (ii) $2Li_2O \rightarrow Li_2O_2 + 2Li^+ + 2e^- \rightarrow O_2 + 4Li^+ + 4e^-$ (the overall reaction, $2O^{2-} \rightarrow O_2 + 4e^-$). The investigation on the mechanism of the O_2 evolution is in progress. The XRD 111 peak intensity of the Co-doped Li_2O was approximately linearly weakened with increase in the charge capacity toward the theoretical capacity of 556 mAh g^{-1} (Figure 4c and Supplementary Figure S4). The upper deviation from the linear line at 540 and 580 mAh g^{-1} is probably due to the O_2 evolution. While the HRTEM image shows fringe regions attributed to Li_2O_2 (Figure 5), the XRD patterns of Co-doped Li_2O upon charged to 270, 324 and 540 mAh g^{-1} showed no Li_2O_2 signal (Supplementary Figure S4) because of the small amount and poor crystallinity. The evolution of CO_2 was not observed in the whole range of the charge process, showing that the Co-doped Li_2O cathode is free from side reactions to produce CO_2 and the superconcentrated LiFSA electrolyte in acetonitrile is stable under the present conditions.

All results demonstrate that the Co-doped Li_2O cathode is charged without the O_2 evolution in the region of 0–216 mAh g^{-1} (Figure 4b) via the oxidation of Co^{2+} to Co^{3+} (0–54 mAh g^{-1}) (Figure 2a) and the subsequent oxidation of O^{2-} to O_2^{2-} (54–216 mAh g^{-1}) (Figure 3a) according to the reaction, $2Li_2O \rightarrow Li_2O_2 + 2Li^+ + 2e^-$: $E^\circ = 2.87$ V. In the higher capacity range, O_2 was evolved, suggesting the progress of reactions with the higher equilibrium potential, $2Li_2O \rightarrow O_2 + 4Li^+ + 4e^-$: $E^\circ = 2.91$ V and/or $Li_2O_2 \rightarrow O_2 + 2Li^+ + 2e^-$: $E^\circ = 2.96$ V as expected thermodynamically. At the present stage, the reversible specific capacity of the Co-doped Li_2O cathode was *ca.* 200 mAh g^{-1} and lower than its theoretical 556 mAh g^{-1}.

In conclusion, we have proposed and demonstrated a new sealed and high-rate battery operating on a redox reaction between O^{2-} and O_2^{2-} with the Co-doped Li_2O cathode and a superconcentrated LiFSA electrolyte in acetonitrile; a reversible capacity over 190 mAh g^{-1}, a high rate capability, and a good cyclability. The reversible capacity was largely dominated by the reaction, $O_2^{2-} + 2e^- \leftrightarrow 2O^{2-}$, with some contribution of the redox reaction of Co. The present specific capacity of the Co-doped Li_2O cathode is still lower than its theoretical 556 mAh g^{-1}. The investigation of roles of Co in the redox reaction between O^{2-} and O_2^{2-} and the state of the O_2^{2-} species in the Co-doped Li_2O would lead to the improvement of the specific capacity.

Methods

Preparation of the Co-Doped Li_2O. Accurately weighed powders of Li_2O (Kojundo Chemical Laboratory co., ltd.) and Co_3O_4 (Wako Pure Chemical Industry, ltd.) were loaded into a zirconia milling pot (45 mL) in an Ar-filled glove box (LABmaster SP, MBRAUN) at atomic ratio of Co/Li = 0.1. The milling pot was fixed in a planetary ball mill machine (Pulverisette 7, Fritsch) and agitated with zirconia milling balls (10 mm diameter × 25) at 600 rpm for 200 h. Then, the milling pot was opened in an Ar-filled glove box and a dark green powder was collected. The elemental analysis of the resulting powder was carried out by inductively coupled plasma atomic emission spectroscopy (ICP-AES); Li 28.7 wt%, Co 24.0 wt%, atomic ratio of Co/Li = 0.099.

Electrochemical Measurements. The Co-doped Li_2O cathode was prepared by blending the active material thoroughly with powder acetylene black and polytetrafluoroethylene at the weight ratio of 45 : 50 : 5. The material was then pressed on an Al mesh (100 mesh) current collector to form an electrode. The cathode, a Li anode pressed on a Cu foil current collector, a concentrated electrolyte solution of 4 M LiFSA in acetonitrile[14], and a glass fibre filter (GA-55, Toyo Roshi Kaisha, Ltd.) as a separator were assembled in two-electrode cells (HS Test Cell or CR2032 coin-type cell, Hosen Corp.). All these procedures were carried out in an Ar-filled glove box. The charge and discharge tests were conducted with a battery charge/discharge system HJ1001SD8 (Hokuto Denko Corporation).

Characterization of Materials. The elemental analysis of Li and Co was performed by ICP-AES with ICPS-8100 (Shimadzu). The Co-doped Li_2O powder (11.37 mg) was weighed in an Ar-filled glove box and dissolved into 1 mL of an aqueous solution (6 M HCl). The solution was diluted in a volumetric flask to 100 mL and then 5 mL of the solution was diluted in a volumetric flask to 50 mL. The concentrations of Li and Co were quantified with standard solutions of Li and Co (0–4 ppm).

Powder XRD patterns were measured using the monochromatized Cu-$K_{\alpha 1}$ radiation on a RIGAKU Smart-Lab system. Every sample was mounted in a gas-tight holder with a Be window filled with Ar. The charged or discharged Co-doped Li_2O cathode was removed from the cell, washed three times with acetonitrile, and dried under vacuum. All procedures were carried out in an Ar-filled glove box.

The oxidation states and coordination environments of Co in the cathode were observed with XANES measurements. The XANES measurements at the Co K-edge were carried out on the BL14B2 beamline at the SPring-8 synchrotron radiation facility (8 GeV, 100 mA) of the Japan Synchrotron Radiation Research Institute (JASRI) in Hyogo, Japan. A Si(111) two-crystal monochromator was used for the measurements of Co K-edge XANES spectra. Ion chambers filled with N_2 (100%) and N_2 (85%)/Ar (15%) were used for the I_0/I detector. XANES spectra at Co K-edge were collected in a transmission mode, and the total acquisition time was 6 min per spectrum. Data reduction was performed by using the REX2000 program (Rigaku Co., Ltd.).

The HRTEM measurements of the Co-doped Li_2O cathode pristine and after charged to 270 mAh g^{-1} were carried out on a JEM-4010 microscope (JEOL, Japan) at an accelerating voltage of 400 kV.

Measurements of O_2 and CO_2 Evolution in the Charging Process. The Co-doped Li_2O cathode (11.3 mg) was pressed on an Al mesh as a current collector. The negative electrode was a metallic Li foil pressed on a Cu mesh. These electrodes, a glass fibre filter separator, and a 4 M LiFSA electrolyte were assembled in a two electrode beaker cell. The resulting beaker cell, a circulation cylinder, and a 2-position 6-port valve with a sampling loop were assembled. All these procedures were carried out in an Ar-filled glove box. Then, the system was transferred outside and connected to the gas flow system directly connected to a quadrupole mass spectrometer (OmniStar GSD301, Pfeiffer Vacuum) (Supplementary Figure S6). The galvanostatic charging test was conducted at a rate of 4.5 mA g^{-1} (50.9 μA) for 168 h at room temperature (*ca.* 298 K) with SI 1287 (Solartron) potentio/galvanostat. The gases in the cell were transferred to the sampling loop by using the circulating cylinder and the analysis was conducted every 12 h with the mass spectrometer as follows: The gases in the sampling loop were purged with a carrier gas (He, 50 mL min^{-1}) by switching the valve and transferred into the mass spectrometer. To remove a vapour of acetonitrile, the purged gases were passed through a cold trap (*ca.* 193 K). The concentrations of O_2 ($m/z = 32$) and CO_2 ($m/z = 44$) were determined with the integrated peak areas of O_2 and CO_2 (with respect to that of Ar ($m/z = 40$)), respectively.

Analysis of Peroxide in Cathodes. The charged or discharged cathodes were removed from the coin-type cell, washed three times with acetonitrile, and dried

under vacuum. Then, the sample, 1 g of ice water in a small glass container frozen with liquid nitrogen at 77 K, and a small amount of Pt powder (<1 mg) were put into the beaker cell (Supplementary Figure S6) and the beaker cell was closed with a gas tight glass cap. The resulting beaker cell, a circulation cylinder, and a 2-position 6-port valve with a sampling loop were assembled. All these procedures were carried out in an Ar-filled glove box. Then, the system was quickly transferred outside and connected to the gas flow system directly connected to a quadrupole mass spectrometer (OmniStar GSD301, Pfeiffer Vacuum) (Supplementary Figure S6). Before the ice melted, the background oxygen concentration in the cell was analysed with the quadrupole mass spectrometer. Then, the sample was dispersed in the ice melting water and O_2 was evolved in the presence of a Pt catalyst. The amount of O_2 evolved was quantitatively estimated with the quadrupole mass spectrometer in the same way as that described in the section of measurements of O_2 and CO_2 evolution in the charging process. It was confirmed in a separate experiment that the amount of Li_2O_2 is quantitatively estimated with the amount of O_2 evolved in the presence of the Pt catalyst according to the reaction, $Li_2O_2 \rightarrow 0.5O_2 + Li_2O$. To confirm the origin of oxygen atoms in the peroxide in the Co-doped Li_2O cathode, the labelled experiment was carried out by using $H_2{}^{18}O$ in an N_2-filled glove box to prevent overlapping of the m/z value of ^{36}Ar with that of $^{18}O_2$. For the mass analysis of the Co-doped Li_2O cathode charged to 270 mAh g^{-1}, a signal at $m/z = 32$ was observed and those at $m/z = 34$ and 36 were not observed (Supplementary Figure S7). These results show that the oxygen atoms in the O_2 result from those in the Co-doped Li_2O cathode.

1. Poizot, P., Laruelle, S., Grugeon, S., Dupont, L. & Tarascon, J-M. Nano-sized transition-metal oxides as negative-electrode materials for lithium-ion batteries. *Nature* **407**, 496–499 (2000).
2. Bervas, M. *et al.* Investigation of the lithiation and delithiation conversion mechanisms of bismuth fluoride nanocomposites. *J. Electrochem. Soc.* **153**, A799–A808 (2006).
3. Badway, F., Pereira, N., Cosandey, F. & Amatucci, G. G. Carbon-metal fluoride nanocomposites structure and electrochemistry of FeF_3:C. *J. Electrochem. Soc.* **150**, A1209–A1218 (2003).
4. Abraham, K. M. & Jiang, Z. A polymer electrolyte-based rechargeable lithium/oxygen battery. *J. Electrochem. Soc.* **143**, 1–5 (1996).
5. Ogasawara, T., Débart, A., Holzapfel, M., Novák, P. & Bruce, P. G. Rechargeable Li_2O_2 electrode for lithium batteries. *J. Am. Chem. Soc.* **128**, 1390–1393 (2006).
6. Zhang, S. S., Foster, D. & Read, J. Discharge characteristic of a non-aqueous electrolyte Li/O_2 battery. *J. Power Sources* **195**, 1235–1240 (2010).
7. Lu, Y.-C., Gasteiger, H. A., Crumlin, E., McGuire, Jr, R. & Shao-Horn, Y. Electrocatalytic activity studies of select metal surfaces and implications in Li-air batteries. *J. Electrochem. Soc.* **157**, A1016–A1025 (2010).
8. Thapa, A. K. & Ishihara, T. Mesoporous α-MnO_2/Pd catalyst air electrode for rechargeable lithium–air battery. *J. Power Sources* **196**, 7016–7020 (2011).
9. Trahan, M. J. *et al.* Cobalt phthalocyanine catalyzed lithium-air batteries. *J. Electrochem. Soc.* **160**, A1577–A1586 (2013).
10. Sathiya, M. *et al.* Reversible anionic redox chemistry in high-capacity layered-oxide electrodes. *Nat. Mater.* **12**, 827–835 (2013).
11. Sathiya, M. *et al.* High performance $Li_2Ru_{1-y}Mn_yO_3$ ($0.2 \leq y \leq 0.8$) cathode materials for rechargeable lithium-ion batteries: Their understanding. *Chem. Mater.* **25**, 1121–1131 (2013).
12. Koga, H. *et al.* Different oxygen redox participation for bulk and surface: A possible global explanation for the cycling mechanism of $Li_{1.20}Mn_{0.54}Co_{0.13}Ni_{0.13}O_2$. *J. Power Sources* **236**, 250–258 (2013).
13. Yoon, W. *et al.* Oxygen contribution on Li-ion intercalation-deintercalation in $LiCoO_2$ investigated by O K-edge and Co L-edge X-ray absorption spectroscopy. *J. Phys. Chem. B* **106**, 2526–2532 (2002).
14. Yamada, Y. *et al.* Unusual stability of acetonitrile-based superconcentrated electrolytes for fast-charging lithium-ion batteries. *J. Am. Chem. Soc.* **136**, 5039–5046 (2014).
15. Antaya, M., Cearns, K., Preston, J. S., Reimers, J. N. & Dahn, J. R. In situ growth of layered, spinel, and rock-salt $LiCoO_2$ by laser ablation deposition. *J. Appl. Phys.* **76**, 2799–2806 (1994).
16. Moen, A. *et al.* X-ray absorption spectroscopic studies at the cobalt *K*-edge on a reduced Al_2O_3-supported rhenium-promoted cobalt Fischer-Tropsch catalyst. *Chem. Mater.* **9**, 1241–1247 (1997).
17. Wu, Z. *et al.* Symmetry dependence of x-ray absorption near-edge structure at the metal *K* edge of 3*d* transition metal compounds. *Appl. Phys. Lett.* **79**, 1918–1920 (2001).
18. Garcia, B., Farcy, J., Pereira-Ramos, J. P. & Baffier, N. Electrochemical properties of low temperature crystallized $LiCoO_2$. *J. Electrochem. Soc.* **144**, 1179–1184 (1997).
19. Narukawa, S. *et al.* Anti-fluorite type Li_6CoO_4, Li_5FeO_4, and Li_6MnO_4 as the cathode for lithium secondary batteries. *Solid State Ionics* **122**, 59–64 (1999).
20. Luge, R. & Hoppe, R. A new cobaltate with isolated anion structure: $Li_6[CoO_4]$. *Z. Anorg. Allg. Chem.* **534**, 61–68 (1986).
21. Pistoia, G., Zane, D. & Zhang, Y. Some aspects of $LiMn_2O_4$ electrochemistry in the 4 volt range. *J. Electrochem. Soc.* **142**, 2551–2557 (1995).
22. Freunberger, S. A. *et al.* Reactions in the rechargeable lithium-O_2 battery with alkyl carbonate electrolytes. *J. Am. Chem. Soc.* **133**, 8040–8047 (2011).
23. McCloskey, B. D., Bethune, D. S., Shelby, R. M., Girishkumar, G. & Luntz, A. C. Solvents' critical role in nonaqueous lithium-oxygen battery electrochemistry. *J. Phys. Chem. Lett.* **2**, 1161–1166 (2011).
24. Ottakam Thotiyl, M. M., Freunberger, S. A., Peng, Z. & Bruce, P. G. The carbon electrode in nonaqueous Li-O_2 cells. *J. Am. Chem. Soc.* **135**, 494–500 (2013).

Acknowledgments

We thank T. Honma and H. Ofuchi (JASRI) for XANES measurements. This work is supported by the Japan Society of the Promotion of Science (JSPS) through its "Funding Program for World-Leading Innovative R&D on Science and Technology (FIRST Program)" and Grants-in-Aid for Scientific Researches from the Ministry of Education, Culture, Sports, Science and Technology.

Author contributions

N.M. conceived the project. S.O., H.O., K.Y. and Y.S. synthesized the material. S.O., Y.O. and Y.S. tested the battery, with direction from M.H., T.K., Y.Y., A.Y. and N.M. S.O. and Y.O. collected and analysed data for X-ray diffraction and X-ray absorption near edge structure measurements, with direction from M.H. and M.O. Y.O. designed and conducted experiments for gas phase analysis and peroxide analysis. E.T. collected and analysed data for electron microscopy, with direction from N.S. and Y.I. N.M. and T.K. supervised the project. S.O., Y.O., M.H., T.K. and N.M. wrote the manuscript.

Additional information

Supplementary information accompanies this paper at http://www.nature.com/scientificreports

Competing financial interests: The authors declare no competing financial interests.

How to cite this article: Okuoka, S.-i. *et al.* A New Sealed Lithium-Peroxide Battery with a Co-Doped Li_2O Cathode in a Superconcentrated Lithium Bis(fluorosulfonyl)amide Electrolyte. *Sci. Rep.* **4**, 5684; DOI:10.1038/srep05684 (2014).